Biochemical and Biophysical Characterization of the Trimerization Domain from the Heat Shock Transcription Factor†

Ralph Peteranderl,[‡,§] Mark Rabenstein,[||,⊥] Yeon-Kyun Shin,[||] Corey W. Liu,[||] David E. Wemmer,[||] David S. King,[‡,#] and Hillary C. M. Nelson*[,‡,▽]

Department of Molecular and Cell Biology and Department of Chemistry, University of California, Berkeley, California 94720, Howard Hughes Medical Institute, and The Johnson Research Foundation and Department of Biochemistry and Biophysics, University of Pennsylvania School of Medicine, Philadelphia, Pennsylvania 19104

Received July 22, 1998; Revised Manuscript Received November 18, 1998

ABSTRACT: Previously, we had characterized a 91 amino acid fragment of the heat shock transcription factor from the yeast *Kluyveromyces lactis* and had shown it to be highly α-helical and sufficient for formation of homotrimers [Peteranderl, R., and Nelson, H. C. M. (1992) *Biochemistry 31*, 12272−12276]. Based on those data, as well as the presence of hydrophobic heptad repeats, we postulated that the trimerization domain contains a three-stranded coiled-coil and that it might resemble the trimerization domain found in influenza hemagglutinin. Here, we further characterize the trimerization domain and show that the minimal domain needs 71 residues to remain trimeric and highly α-helical. ^{19}F NMR spectroscopy suggests that the structure contains three parallel strands that are in register along the long axis of the coiled-coil. Electron paramagnetic resonance spectroscopy studies show that the C-termini of the subunits are in close proximity; this is in contrast to the topology of the hemaglutinin trimerization domain where the C-termini form buttressing helices. Analytical ultracentrifugation also confirms that the structure is elongated and unlikely to have buttressing helices. Additional experiments suggest that the trimerization domain has at least two subdomains. The first subdomain has the potential to form trimers independently, though not as stably as the complete domain. The second subdomain is quite helical, forms large oligomers, and appears to provide stability to the complete domain. Our current model for the heat shock transcription factor trimerization domain is a highly elongated coiled-coil structure, with a potential break in the coiled-coil region located between the two subdomains.

Cells react to physiological and environmental stresses through a conserved mechanism called the heat shock, or stress, response. In eukaryotic cells, this response is controlled at the transcriptional level through a specific transcriptional activator called the heat shock transcription factor (HSF) (*1*). The number of HSF homologues, as well as their overall sequence and length, varies from species to species, but there are two main conserved regions, the DNA binding domain and the oligomerization domain. The DNA binding domain recognizes a conserved DNA sequence motif, the heat shock element (HSE). HSEs contain varying numbers of the DNA sequence NGAAN in alternating inverted repeats (*2*, *3*). Although HSF will bind to a two-repeat HSE in vitro, at least three repeats are necessary for activity in vivo. The oligomerization domain allows HSF to form trimers; HSF is unique in that it functions as a sequence-specific homotrimeric DNA binding protein. The adaptive advantage conferred by binding as a trimer is not clear at this point. The presence of three DNA binding domains might be necessary to increase the affinity for the DNA binding site (*4*), but the trimeric nature of HSF could also be a consequence of the requirements of other aspects of HSF's regulation and function, a suggestion made because of the extensive conservation found between trimer domains across the eukaryotic kingdom, especially in residues not directly involved in the trimeric interface (*5*). In higher eukaryotes, for example, the trimerization domain appears to be involved in the regulation of HSF activity (*1*, *6*): under nonstress conditions, HSF is monomeric and is located in the cytoplasm, while upon stress, the protein trimerizes and translocates to the nucleus (*7*, *8*). This behavior is not universal, however, and in budding yeasts such as *Saccharomyces cerevisiae* and *Kluyveromyces lactis*, HSF appears to be trimeric and located in the nucleus under all conditions (*9*, *10*).

† This work was supported in part by U.S. Public Health Service Grant GM-44086 (to H.C.M.N.), as well as by U.S. Public Health Service Grant GM-51290 (to Y.-K.S.), NIH Traineeship Grant GM-08295 (to C.W.L.), the Director, Office of Energy Research, through the Office of Biological and Environmental Research of the U.S. Department of Energy under Contract DE-AC03-76SF00098 (to D.E.W.), and through instrumentation grants from the U.S. Department of Energy (DEFG05-86ER75281) and the National Science Foundation (DMB 86-09305) and BBS Grant 87-20134 (to D.E.W.).

* Address correspondence to this author at the Department of Biochemistry and Biophysics, University of Pennsylvania School of Medicine, A501 Richards Building, 3700 Hamilton Walk, Philadelphia, PA 19104-6089.

‡ Department of Molecular and Cell Biology, University of California, Berkeley.

§ Present address: Department of Biochemistry and Biophysics, University of California, San Francisco, CA 94143.

|| Department of Chemistry, University of California, Berkeley.

⊥ Present address: Department of Molecular and Cell Biology, University of California, Berkeley, CA 94720.

Howard Hughes Medical Institute.

▽ University of Pennsylvania School of Medicine.

10.1021/bi981774j CCC: $18.00
Published on Web 03/05/1999

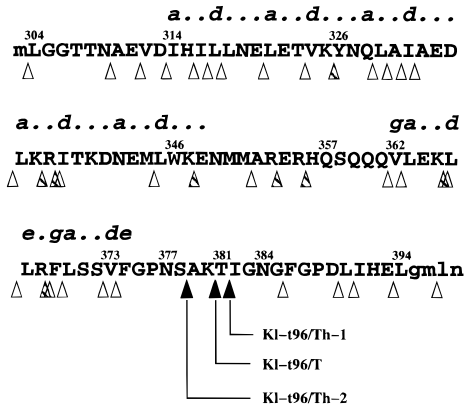

FIGURE 1: Proteolysis of trimerization domain. The sequence of Kl-t96 is shown, with the residues introduced during cloning (see Materials and Methods) marked in lower-case letters. Positions *a* and *d* of the heptad repeats in helix A, as well as positions *a*, *d*, *e*, and *g* of the overlapping heptad repeats in helix B, are indicated above the sequence. The potential recognition sites for trypsin and thermolysin are indicated by open and cross-hatched triangles, respectively. The black triangles mark the C-termini of the stable proteolytic fragments that could be isolated, including Kl-t96/Th1 and Kl-t96-Th2 from the thermolysin digestion and Kl-t96/T from the trypsin digestion.

Previous studies had shown that a region of approximately 100 residues located within the center of the protein is necessary and sufficient for the trimerization of yeast HSF (*11*). Based on the high α-helical content as measured by circular dichroism (CD) spectroscopy, as well as the presence of hydrophobic heptad repeats, we had proposed that the trimerization domain forms a three-stranded coiled-coil (*5*). Further inspection of the sequence within this region showed heptad repeats occurring in two subdomains (Figure 1): helix A or HR A, located at the N-terminus of the trimerization domain around residues 314−348 of the *K. lactis* HSF; and helix B or HR B, located at the C-terminus of the domain around residues 362−373 (*11*−*13*). Helix A appears to be an amphiphilic helix with a heptad repeat that contains a distribution of nonbranched residues in position *a* and *β*-branched residues in position *d* of the heptad repeat '*abcdefg*', which is typical for trimeric coiled-coils (*14, 15*). Helix B, also a putative amphiphilic helix, contains hydrophobic residues at positions *a*, *d*, *e*, and *g* (using the heptad repeat of helix A as a reference). Because of the two overlapping frames of the hydrophobic repeats, it is not immediately clear from the sequence whether helix B forms a coiled-coil, and, if so, which set of residues would form the hydrophobic interface between helices. Helices A and B are connected by a series of polar, bulky residues with a low potential for the formation of a coiled-coil, yet this connecting region has a high degree of conservation, suggesting an important role in the function of the trimerization domain.

Based on sequence considerations as well as our previous results (*5*), a number of possible models for the overall fold of the trimerization domain can be proposed. In these models, the orientation of the subunits and the roles of helices A and B are the major variables. First, the orientation of the subunits could either be all-parallel or be two-parrallel/one-antiparallel. Structural examples exist for both types of three-stranded coiled-coils (*14, 16*−*20*). Second, the roles of helices A and B need to be addressed. Is the structure one long continuous helix? Or, do helices A and B both form coiled-coils separated by a loop, as found in the structure of T4 fibritin (*20*)? Or, is one of the helices involved in other tertiary structure elements, such as the formation of a buttressing helix, as found in viral envelope glycoproteins (*16, 21*)?

Table 1: Summary of Proteins

name	residues	name	residues
Kl-t96	L304−L394	Kl-t65	I314−V373
Kl-t86	L304−N384	Kl-t59	L304−V362
Kl-t83	L304−T381	pepC3	Q357−N377
Kl-t75	L304−V373		

In this paper, we present the results of our continued attempts to elucidate the structure of the trimerization domain from *K. lactis* HSF. The boundaries of the trimerization domain have been further defined, and the subdomains (helices A and B) have been analyzed. A series of spectroscopic approaches has been used to address questions about the overall topology of the domain. From these experiments, we show that the isolated HSF trimerization domain forms an all-parallel, elongated structure.

MATERIALS AND METHODS

Cloning and Site-Directed Mutagenesis. The overexpression vectors used are based on the T7 expression plasmids described previously for the overexpression of the trimerization domain of *K. lactis* HSF (*5, 12, 22*). A summary of the proteins used in this study is given in Table 1. N-Terminal and C-terminal truncations were made by introducing *Nde*1 and *Sph*I sites, respectively, by site-directed mutagenesis protocols (*23*). The expressed proteins all include an N-terminal methionine residue and, unless stated otherwise, include the C-terminal tetrapeptide GMLN, which was introduced by the expression vector. The trimerization domain is represented by residues L304 through L394 of *K. lactis* HSF for Kl-t96, residues L304 through N384 for Kl-t86, residues L304 through T381 for Kl-t83, residues L304 through V373 for Kl-t75, and residues I314 through V373 for Kl-t65. Kl-t59 was constructed by replacing the codon for residue V362 at the beginning of helix B with a stop codon and contains residues L304 through Q361 without the C-terminal tetrapeptide GMLN. The mutant Kl-t75 W346C was constructed by standard protocols from Kl-t75. A C-terminal cysteine residue (cC) was introduced by making use of an alternative expression vector backbone in which the C-terminal tetrapeptide GMLN was replaced by the sequence GMLC (*4, 24*), creating the proteins Kl-t75 cC, with a cysteine residue at the C-terminus of the protein, and Kl-t75 W346C/cC, with one cysteine residue at the C-terminus of the protein and an additional cysteine residue at position 346. The mutants Kl-t75 z2bg and Kl-t75 z2,3bg, which remove the coiled-coil repeats in the C-terminus of Kl-t75 and change the sequence from VLEKLLRFLSSVG-MLN to VNEKQLRFNSSNGMLN and ANEKQYRYNSS-NGMLN, respectively, were constructed by standard protocols from Kl-t75.

Protein Overexpression and Purification. The *E. coli* strain BL21(DE3)/pACYC177LacI^{Q} was freshly transformed with the respective expression plasmids for protein expression.

For standard constructs, cells were grown in Terrific Broth (TB) medium (*25*) at 37 °C while shaking until they reached an $A_{600\ nm}$ of approximately 0.4. At that point, expression was induced by addition of isopropyl β-D-thiogalactopyranoside (IPTG) to a final concentration of 2 mM. Incubation was continued at 37 °C for 1 h, after which rifampicin was added to a final concentration 0.25 μg/mL. The cells were then transferred to 25 °C and incubated overnight while shaking. The cells were harvested by centrifugation for 10 min at 4000*g* (7 °C). The cell pellet was resuspended in 0.1 volume of ice-cold isotonic buffer (50 mM Tris-HCl, pH 7.5, 150 mM NaCl, 2 mM EDTA). The cell suspension from 1.6 L of cells was pooled and centrifuged again (10 min at 4000*g*, 7 °C). The resulting pellet (typically 5−7 g wet weight) was resuspended by stirring and repeated pipetting in 10 mL of RB200 [50 mM Hepes, pH 8.0, 200 mM NaCl, 5 mM $CaCl_2$, 2 mM EDTA, 10% (v/v) glycerol], and then frozen at −70 °C.

In the standard purification protocol, the frozen cells were thawed on ice and lysis was started by addition of 10 mL of ice-cold RB200 with 2 mg/mL hen egg white lysozyme, 2 mM phenylmethanesulfonyl fluoride (PMSF), 2 μg/mL aprotinin, 4 μg/mL leupeptin, and 2 μg/mL pepstatin. The thawing cells were kept on ice for 30 min, with gentle mixing by inversion every 10 min. The cells were sonified with a Branson Sonifier 250 until the viscosity of the cell suspension dropped by about 90%. The suspension was then centrifuged at 30000*g* for 30 min at 7 °C. The supernatant was transferred to a new centrifuge tube, saturated $(NH_4)_2SO_4$ was added to a final concentration of 30% (v/v), and the mixture was incubated on ice for 30 min. The precipitate was collected by centrifugation at 12000*g* for 30 min at 7 °C. The pellet was dissolved in 30 mL of ice-cold RB200 and diluted with an equal volume of 2× column loading buffer [50 mM Hepes, pH 8.0, 200 mM NaCl, 1200 mM $(NH_4)_2SO_4$]. The subsequent chromatographic and dialysis steps were all performed at room temperature. The first two chromatographic steps were done on a Waters 650 Advanced Protein Purification System, while the last chromatographic step was done on a Waters HPLC. The solution was loaded onto a hydrophobic interaction chromatography column (100 × 25 mm i.d., SynChropak Propyl, 300-Å pore size), equilibrated with 50 mM Hepes, pH 8.0, 200 mM NaCl, 600 mM $(NH_4)_2SO_4$. The column was developed in a linear gradient over 30 min to 50 mM Hepes, pH 8.0. The protein typically eluted around 150 mM $(NH_4)_2SO_4$, 50 mM NaCl. The fractions containing the protein were pooled and dialyzed against two changes of 2 L of 50 mM Tris, pH 8.8, 100 mM NaCl. After dialysis, the protein solution was diluted 2.5-fold with buffer to 50 mM Tris, pH 8.8, 40 mM NaCl, and loaded onto an anion-exchange chromatographic column (100 × 10 mm i.d., Waters Accell Plus QMA, 500-Å pore size, 50-μm average particle size), equilibrated in 50 mM Tris, pH 8.8, 40 mM NaCl. The column was developed over 30 min in a linear gradient to 50 mM Tris, pH 8.8, 1000 mM NaCl. The protein eluted as the main peak around 400 mM NaCl. The fractions containing the protein were pooled and loaded on a Vydac C18 column (250 × 10 mm i.d., 300-Å pore size, 10-μm particle size, Separations Group), equilibrated to 10% acetonitrile, 0.09% trifluoroacetic acid (TFA) in water. The column was brought to 40% acetonitrile, 0.06% TFA in 2 min, and then developed over 30 min to 50% acetonitrile, 0.05% TFA. The protein eluted around 57% acetonitrile; identity and purity of the sample were confirmed by electrospray ionization mass spectrometry (ESI-MS; Hewlett-Packard 5989A); all masses were found to be within 0.5 amu of the calculated masses.

Kl-t59 was expressed as described above. However, it was precipitated from the crude cell lysate after sonification with 20% (v/v) ethanol on ice for 30 min. The precipitate was collected by centrifugation at 12000*g* for 30 min at 7 °C, and subsequently redissolved in 20 mL of RB200. The protein was precipitated at 4 °C by addition of saturated $(NH_4)_2SO_4$ to 45% (v/v). The pellet was dissolved in column buffer and loaded onto the hydrophobic interaction chromatographic column. The fractions containing the protein were loaded directly onto the reversed-phase HPLC column, and the protein was purified as described above.

Cysteine-containing mutants for the electron paramagnetic resonance experiments were purified through a slightly modified protocol. Induction, harvesting, and lysis of the cells were done as described above. However, in the steps that followed great care was taken to maintain reducing conditions. Dithiothreitol was added to a final concentration of 10 mM both after lysis and again after the resuspension of the $(NH_4)_2SO_4$ pellet in RB200. In addition, sodium tetrathionate was added to a final concentration of 2 mM to the dialysis buffer and all the running buffers for the hydrophobic interaction and anion-exchange chromatographic columns.

^{19}F-labeled protein was expressed through a modified version of the standard protocol. Cells were grown in supplemented M9 medium [6 g/L Na_2HPO_4, 3 g/L K_2HPO_4, 1 g/L NH_4Cl, 0.5 g/L NaCl, 1 mM $MgCl_2$, 0.4% (v/v) glycerol, 0.04 g/L of each of the 20 L-amino acids]. Cells were grown at 37 °C while shaking until they reached an $A_{600\ nm}$ of approximately 0.4. They were then harvested by centrifugation at 4000*g* for 10 min at room temperature. The cell pellets were then resuspended in prewarmed supplemented M9 minimal medium, in which either tyrosine or tryptophan was replaced by 0.1 g/L of a racemic mixture of D- and L-*m*-fluorotyrosine or 5-fluorotryptophan, respectively. Incubation was continued for another 30 min at 37 °C. The cultures were then induced by adding IPTG to a final concentration of 2 mM, followed by an additional 60 min of incubation at 37 °C. At this point, rifampicin was added to a final concentration of 0.25 μg/mL, and the cells were incubated for another 8 h at 25 °C. Lysis and protein purification were done as described above. Incorporation of the fluorinated amino acids as determined by ESI-MS was around 50% for *m*-fluorotyrosine and around 75% for 5-fluorotryptophan.

Protein concentration was determined by absorption at 280 nm. The extinction factor was calculated to be around 7000 mol^{-1} cm^{-2} for all proteins with the exception of Kl-t75 W346C and Kl-t75 z2,3bg, based on the sequence of the protein. For Kl-t75 W346C and Kl-t75 z2,3bg, extinction coefficients of 1300 mol^{-1} cm^{-2} and 9600 mol^{-1} cm^{-2} were used. Since no difference was seen in the absorption of the native and unfolded protein, all concentration determinations were done under native conditions.

Peptide Synthesis. Peptides were synthesized using standard 9-fluorenylmethoxycarbonyl chemistry (Fmoc) on an Applied Biosystems ABI 431 A peptide synthesizer. Cleavage and deprotection followed established protocols (*26*). The

peptide pepC3 (Ac-QSQQQVLEKLLRFLSSVFGPNY-NH_2), corresponding to the C-terminal end of the *K. lactis* trimerization domain (residues Q357 through N377), also included a tyrosine residue at the C-terminus to facilitate detection. This peptide synthesized as a C-terminal amide and acetylated at the N-terminus. All peptides were checked by ESI-MS. An extinction coefficient of 1300 mol^{-1} cm^{-2} was used to determine the protein concentration for pepC3.

Limited Proteolysis. Initial tests were done at a mass ratio of 1:100 for protease and Kl-t96. The proteases screened were trypsin, chymotrypsin, Pronase, thermolysin, papain, and ficin. Reactions of 100 μL volume were incubated at 37 °C, and 25 μL aliquots were removed at 0, 15, 30, and 60 min. The reactions were stopped by boiling in SDS−PAGE loading buffer, and the proteolysis products were analyzed by SDS−PAGE.

Based on the initial screening, proteolysis experiments on a preparative scale were done with thermolysin and trypsin. Kl-t96 (10 mg) was dissolved in 10 mL of 25 mM sodium phosphate buffer, pH 8.8, 100 mM NaCl. The protein was incubated at 37 °C with 100 μL of 1 mg/mL trypsin or thermolysin. Aliquots (2 mL) were removed at 4, 8, and 60 min, and the reactions were stopped by addition of 20 μL of 10% TFA in water. Proteolysis products were separated on a reversed-phase HPLC column as described above, with detection at 230 nm. The N-termini of the main fragments were identified by N-terminal sequencing; the C-termini were derived from the mass of the fragments as determined by ESI-MS.

Circular Dichroism Spectroscopy. Circular dichroism (CD) spectra were recorded on an AVIV 62DS spectropolarimeter with a 2 mm strain-free quartz cuvette (Hellma). Proteins were dialyzed extensively into one of two buffers: sodium/phosphate (Na/P) buffer, pH 8.8, or citrate/phosphate (C/P) buffer, pH 8.0 (19.54 mM Na_2HPO_4, 0.275 mM citric acid). Spectra were recorded at 25 °C in 1 nm steps with a time constant of 15 s. Thermal melts were done at a protein concentration of 20 μM (monomer) with detection at a wavelength of 222 nm unless stated otherwise. The temperature was increased in 2 °C steps with a 2 min equilibration and a time constant of 15 s. Reversibility of the thermal melts was monitored via the reappearance of the initial ellipticity of the sample upon return to the starting temperature and the constant optical transmission throughout the thermal melt. Since not all the fragments melted reversibly under the given conditions, 1 M guanidinium chloride was added to prevent aggregation of the denatured protein where noted. Fractional helicity was estimated based on the empirical formula $f_H = -(\theta_{222} + 2340)/30300$ (*27*).

^{19}F NMR Spectroscopy. ^{19}F NMR spectra were collected on a General Electric Omega 500 NMR spectrometer with an inverted proton probe tuned to 470 MHz. The lyophilized ^{19}F-labeled proteins were resuspended in H_2O and roughly neutralized by addition of 1 M NaOH using the reversible precipitation of the proteins at the isoelectric point (pH 6.5) as an indicator for the amount of base necessary to compensate for the TFA carried over from the HPLC step. The protein was buffered to pH 8 by addition of 10× C/P buffer stock to make the final solution 1× C/P. The final sample volume was 0.5 mL (90:10 H_2O:D_2O), and protein concentrations were approximately 0.75 mM and 0.9 mM for the fY326 and fW346 samples, respectively. A total of 4000 transients were acquired per sample with a 15 μs 90° pulse, a spectral width of 12 000 Hz, and a 1 s relaxation delay between scans. A 10 Hz exponential line broadening was applied to the time domain data prior to Fourier transformation. A fifth-order polynomial correction was applied to the frequency domain data to flatten the base line. Chemical shifts were referenced to a 10% aqueous solution of TFA (set to 0 ppm).

Spin-Labeling of the Cysteine-Containing Mutants. Reduced lyophilized protein was dissolved in H_2O; residual TFA from the HPLC purification lowered the pH far enough to prevent accidental oxidation at this point. A small aliquot was removed and used to determine the protein concentration at pH 8. A 3-fold excess of 3-(2-iodoacetamido)-2,2,5,5-tetramethyl-1-pyrrolidinyloxyl (IAAP) was added to the acidic protein solution. The labeling reaction was started by adjusting the pH of the sample approximately to neutrality with 10× C/P buffer (194.5 mM NaH_2PO_4, 2.75 mM citric acid, pH 8.0), using the reversible precipitation of the proteins at the isoelectric point (pH 6.5) as an indicator for the amount of buffer stock necessary to compensate for the TFA carried over from the HPLC step. The labeling reaction was incubated for 2 h at room temperature. The labeled protein was purified by reversed-phase HPLC as described above, and the purity of the protein as well as the efficiency of the labeling reaction were determined by ESI-MS. The correct fractions were lyophilized and stored at −20 °C. Prior to analysis, the labeled protein was dissolved in 5 mL of H_2O, and the pH was adjusted to roughly neutrality by addition of 1 M NaOH and then buffered to pH 8 by addition of 10× C/P buffer stock to make the final solution 1× C/P. The volume was then reduced to 100 μL by ultrafiltration. Secondary structure and stability were determined by CD spectroscopy as described above.

Electron Paramagnetic Resonance Measurements. Electron paramagnetic resonance (EPR) spectra were recorded on a Bruker ESP 300 EPR spectrometer with a loop−gap resonator. The resonator frequency was 9.77 GHz. Samples were flash-frozen in an acetone/dry ice bath and then cooled in a cold nitrogen stream (−142 °C). The low-temperature spectra were recorded as a first derivative of the signal over a magnetic field sweep of 150 G with a modulation amplitude of 2.09 G. In experiments where heterotrimers with only a single labeled subunit were used, a 30-fold excess of unlabeled wild-type protein was added. As a standard for noninteracting spins, pure IAAP in 10% (v/v) glycerol was used.

Analytical Ultracentrifugation. All experiments were done using a Beckman XL-A analytical ultracentrifuge. All experiments were done in C/P buffer, and the density (ρ = 0.998 g cm^{-1}) and viscosity (η = 0.01002 g cm^{-1} s^{-1}) of the solvent were calculated based on standard tables (*28*). Sedimentation velocity experiments for Kl-t75 were done at 25 °C and 60 000 rpm. Hydration was assumed to be 0.25 g of H_2O/g of protein (*29*). Sedimentation equilibrium experiments were done at a range of starting proteins concentrations from 2 to 100 μM and speeds from 30 000 to 50 000 rpm, with temperatures of 15 °C for Kl-t75 and Kl-t59 and 5 °C for pepC3 and the Kl-t75 mutants. After equilibrium was established, the concentration gradient was determined by the absorption at 280 nm for all proteins with the exception of pepC3, where it was determined at 222 nm.

The data were analyzed using the data analysis program IGORPRO (Wavemetrics, Inc.), which has been adapted for analyzing XLA data based on early work by Henlsey and colleagues (*30*) and refined by James D. Lear. Dissociation constants were calculated by fitting the data to different equilibria models; because of uncertainties in the measurements and the calculated models, we estimate that the dissociation constants are only accurate to within approximately 10% of their value. For Kl-t59, the data were extremely well described by a monomer−trimer equilibrium. Analysis with a monomer−dimer−trimer equilibrium led to undetectable (less than 2%) concentrations of a dimeric species, no changes in the residuals, and no significant differences in the apparent monomer−trimer dissociation constant. For Kl-t75, the data were best fit by a monomer−trimer−hexamer equilibrium. Addition of a dimeric species led to low (less than 8%) concentrations of a dimeric species, again with no changes in the residuals and no significant differences in the apparent monomer−trimer or trimer−hexamer dissociation constants. Because pepC3 aggregates to a large oligomer, the data were fit to a fixed molecular weight with no attempt at guessing equilibria models.

RESULTS

Defining the Boundaries of the Trimerization Domain. The initial boundaries of the HSF trimerization domain were defined by studies of expressed fragments of *S. cerevisiae* HSF (*11*), in combination with sequence comparisons between HSFs (*5*). This lead to our previous choice of the fragment Kl-t96 for our studies, which contains residues 304−394 from *K. lactis* HSF (*5*). In the present study, we used limited proteolysis of Kl-t96 as a first step to narrow down the functional boundaries of the trimerization domain. This approach makes use of the fact that the parts of a polypeptide sequence that are not folded into a domain are more susceptible to degradation by proteases. Treatment of Kl-t96 with trypsin gave rise to a large, stable fragment (called Kl-t96/T), which could be purified by HPLC. The main product of treatment with thermolysin was fragment Kl-t96/Th1, which over time was further cleaved to yield Kl-t96/Th2; both fragments were also easily purified by HPLC. All three fragments are largely α-helical as determined by CD spectroscopy and form trimers as assayed by chemical cross-linking (data not shown). Analysis of the proteolytic fragments by ESI-MS and Edman sequencing showed that all three fragments retain the original N-terminus of the protein, with cleavage occurring C-terminal to the following residues: S378 for Kl-t96/Th2, K380 for Kl-t96/T; and T381 for Kl-t96/Th1 (Figure 1). A large number of potential cleavage sites in the sequence are not recognized by the proteases, suggesting that these parts of the polypeptide chain form a stable structure which protects the sites from cleavage. In particular, three putative thermolysin sites in the N-terminal part of the protein, located after residues 308, 310, and 312 upstream of the start of the heptad repeat of helix A, are protected from cleavage. This suggests that the N-terminal boundary of the trimerization domain extends considerably beyond the heptad repeat.

Using the results from limited proteolysis in conjunction with the location of the heptad repeats, we expressed three new fragments of *K. lactis* HSF: Kl-t86 (residues L304−N384), Kl-t83 (residues L304−T381), and Kl-t75 (L304−V373). As predicted, all three truncations are highly α-helical and form trimers as assayed by chemical cross-linking and analytical ultracentrifugation (data not shown). Comparison of the CD spectra for Kl-t75 and Kl-t96 shows a higher average helicity per residue for Kl-t75 than Kl-t96 (Figure 2A), although the thermal melting point of Kl-t75 is approximately 10 °C lower than Kl-t96 under identical conditions (data not shown). Truncations in the N-terminal region had considerably more dramatic consequences. Kl-t65, a version of Kl-t75 in which the N-terminal 10 residues upstream of the heptad repeat in helix A have been removed, shows essentially no helicity (Figure 2B), again suggesting an important role for the N-terminal sequence.

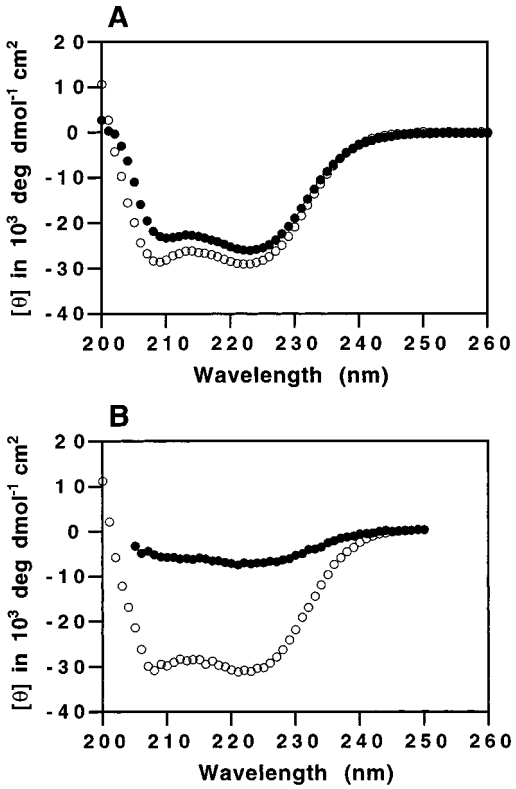

FIGURE 2: Secondary structure of constructs. (A) Circular dichroism spectra of Kl-t75 (○) shown in comparison to Kl-t96 (●) at 50 μM in 25 mM sodium phosphate, pH 8.8. (B) Circular dichroism spectra for Kl-t65 (●) shown in comparison to Kl-t75 (○) at 20 μM in C/P buffer. Note that Kl-t75 has similar spectra in the two different buffers.

These experimental results were used in conjunction with sequence analysis to choose the appropriate fragment for further study. V373 is found at the end of one of the potential heptad repeats in helix B, and it is followed by residues in the HSF sequence (FGP...) with low helical propensities. As V373 is the last residue in the Kl-t75 fragment, we selected Kl-t75, which includes residues L304 through V373, as the minimal trimerization domain to be used for further physical studies.

Orientation of the Strands. Our initial results had suggested that the HSF trimerization domain most likely forms a three-stranded coiled-coil. However, the question remained whether this coiled-coil is composed of parallel helices, or whether one of the three strands is oriented in an antiparallel fashion, as observed in the structure of spectrin (*17*) or in the case of a synthetic three-helix bundle (*18*). To discriminate between

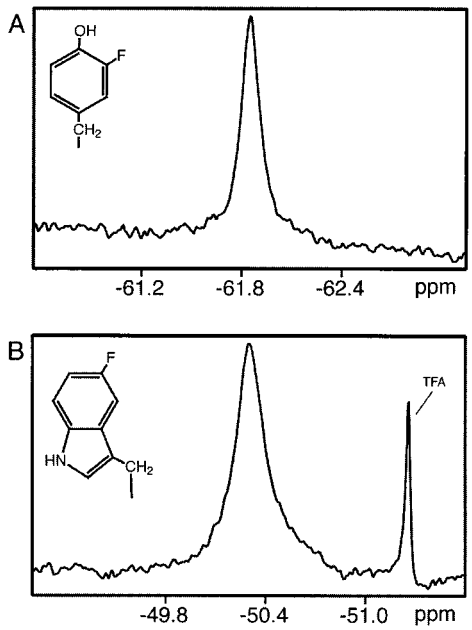

FIGURE 3: ^{19}F NMR spectra for Kl-t75 labeled at Y326 and W346. In two independent experiments, fluorinated amino acid analogues were incorporated into Kl-t75 at (A) position Y326 and (B) position W346. The positions fluorinated are indicated on the structures. In both cases, ^{19}F NMR spectra detect only a single resonance for the introduced fluorine nucleus. The additional sharp peak in (B) is residual TFA that has been folded into this spectral range due to digitization.

these two possibilities, we used ^{19}F NMR spectroscopy of fluorinated forms of the protein (Figure 3). Analogues of either tyrosine or tryptophan were incorporated at a single site of the protein (fY326 or fW346, at positions *f* or *e*, respectively, of the heptad repeat). The chemical shifts of heavier nuclei, such as ^{19}F, are strongly influenced by environment, and therefore by charged groups in their proximity. The trimers with fluorinated residues in either position show only a single chemical shift, indicating that in both cases the residues in all three subunits are found in a single environment, an observation consistent only with a parallel trimeric structure. The line widths for fY326 and fW346 are slightly larger (52 and 64 Hz, respectively) than the 40 Hz for a protein of similar molecular mass on the spectrometer used. This line broadening was also observed in proton spectra of the trimerization domain, and is most likely due to the effect of slow tumbling of the long axis in a rather asymmetric molecule.

Inter- and Intrasubunit Distances. We employed electron paramagnetic resonance (EPR) spectroscopy to determine inter- and intrasubunit distances in the trimer. Since the *K. lactis* HSF trimerization domain contains no naturally occurring cysteine residues, we introduced cysteines at specific sites and used these cysteines to label the protein quantitatively with the thiol-specific nitroxide-based spin-label IAAP. The spin-labeled proteins show α-helicity, stability, and oligomerization properties similar to the wild-type protein, as determined by CD spectroscopy and chemical cross-linking (data not shown). EPR spectroscopy measures the interactions between unpaired electrons, and can be used to determine distances in the 8−25 Å range (*31*). EPR measurements were taken at room temperature, where the isotropic spin exchange interactions can be observed out to

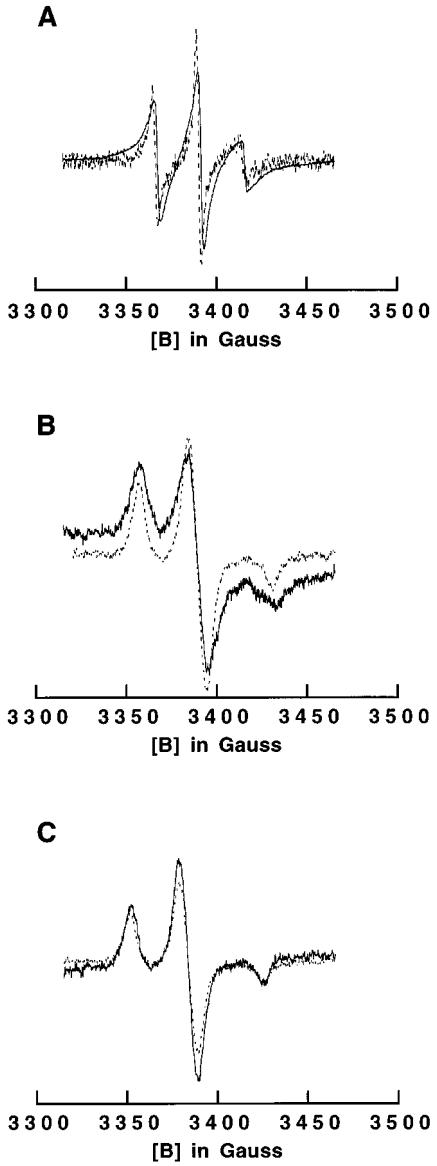

FIGURE 4: Electron paramagnetic resonance spectra of proxyl-labeled Kl-t75. (A) Intersubunit interactions at room temperature. Kl-t75 cC was labeled at the C-terminus with a proxyl group (IAAP), and the spectrum of homotrimeric Kl-t75 cc-IAAP (solid line) was recorded. For comparison, a spectrum was taken of a heterotrimeric sample (dashed line), in which Kl-t75 cc-IAAP was mixed with a 30-fold excess of unlabeled Kl-t75 to ensure that all trimers had only a single C-terminal spin-label. (B) Intersubunit interactions at low temperature. Kl-t75 Cc was labeled at the C-terminus with a proxyl group (IAAP). The spectrum of the Kl-t75 cC−IAAP homotrimer (solid line) was recorded at −140 °C and compared to the spectra of IAAP alone (dashed line). (C) Intrasubunit interactions. Kl-t75 W346C/Cc was labeled with IAAP at both cysteine residues and mixed with a 30-fold excess of unlabeled Kl-t75. The spectrum of this heterotrimer (solid line) was compared to the spectrum of a IAAP solution (dashed line). Spectra were recorded at −140 °C.

∼15 Å, as well as at low temperatures, where the anisotropic dipole−dipole interactions can be observed quantitatively out to 25 Å.

Intersubunit distances were measured using a C-terminally labeled derivative of Kl-t75 (Kl-t75 cC). First, an EPR spectrum was taken at room temperature for a heterotrimeric mixture of C-terminally labeled subunits and a 30-fold excess of unlabeled protein (Figure 4A). This heterotrimeric mixture

ensures that most of the proteins have zero or one spin-label. The resulting spectrum is typical for a molecule with a very short correlation time, showing little or no line broadening at room temperature. This indicates that the spin-label is rotating freely in the solvent (*32*) and the C-terminus is free of interactions with one another, rather than being tightly packed in an interface between the three subunits. The room-temperature spectrum of the labeled homotrimer, on the other hand, shows some line broadening compared to the spectrum of the single-labeled heterotrimer (Figure 4A). This observation implies interactions between spin-labels, indicating they are in close (∼10 Å) proximity. To follow up on these qualitative results, we recorded low-temperature spectra at −140 °C (Figure 4B) in order to reduce the motions of the protein that might interfere with detection of the interactions. If the low-temperature spectrum of the labeled homotrimer is compared to a set of standard spectra for spin-labels at a known distance (*31*), it is most similar to the spectrum of two labels separated by 10.8 Å. This roughly corresponds to a distance of 13−14 Å between proxyl groups within the trimer.

We measured intrasubunit distances by using the doubly labeled derivative of Kl-t75 (Kl-t75 W346C/cC) along with an excess of unlabeled protein to ensure that all the observed interactions came from trimers with only a single labeled subunit. The spectrum was compared to free IAAP to compare line widths and shapes. No interactions are observed for the heterotrimer at low temperature (Figure 4C) or room temperature (data not shown), indicating that the two labels must be separated by more than 25 Å in the subunit. This supports the hypothesis of an elongated structure for the trimerization domain.

Sedimentation Velocity Measurements and Modeling. Shape information can be obtained from sedimentation velocity experiments by knowing the molecular weight and estimating the hydration shell and partial specific volume. The sedimentation coefficient ($s_{20,w}$) for Kl-t75 was determined to be 2.25 S (data not shown). We can use this value, along with the molecular weight, to calculate a frictional coefficient, f, of 5.05×10^{-8} g s^{-1}. Assuming a hydration shell of 0.25 g of H_2O/g of protein and a partial specific volume of 0.73 cm^3 g^{-1}, we can calculate a hydrated volume of 43.1 nm^3, which leads to a hydrated radius, r_h, of 21.75 Å for a sphere. This can be used to obtain a spherical frictional coefficient, f_{sph}, of 4.11×10^{-8} g s^{-1}. The ratio of the observed frictional coefficient to the calculated spherical frictional coefficient gives a value F, called the Perrin value, of 1.22. Assuming that Kl-t75 forms a prolate ellipsoid, we can use the Perrin value to estimate a semi-axial ratio of close to 1:5 (*33*). This ratio also supports our model of an elongated structure for the trimerization domain.

Analysis of Subdomains. The functions of the two postulated subdomains of the trimerization domain, helices A and B, were initially analyzed by studying them in their isolated form. Helix A, the N-terminal part of the domain, is represented by the protein Kl-t59, which was designed to include the complete helix A as well as the region between helices A and B. Kl-t59 has approximately 40% helical content under standard conditions, while peptides lacking this region between helices A and B are considerably less helical (data not shown). The oligomerization state of Kl-t59 in solution was determined by sedimentation equilibrium

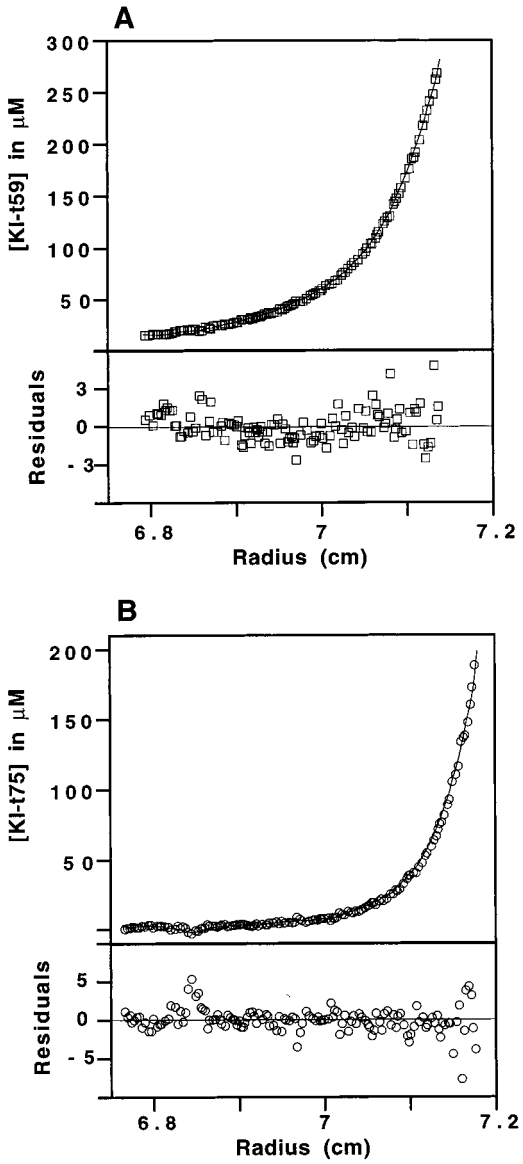

FIGURE 5: Oligomerization states of Kl-t59 and Kl-t75. (A) The concentration gradient of Kl-t59 at sedimentation equilibrium is shown with a starting condition of 20 μM and speed of 30 000 rpm. Residuals were calculated for a global fit at three speeds (30 000, 40 000, and 50 000 rpm) to a monomer−trimer equilibrium. For clarity, only every other data point is shown. (B) The concentration gradient of Kl-t75 at sedimentation equilibrium is shown with a starting condition of 100 μM and speed of 30 000 rpm. Residuals were calculated for a global fit of two runs (only one of which is shown here) to a monomer−trimer−hexamer equilibrium. For clarity, only every other data point is shown.

centrifugation. The observed concentration gradient of the protein agrees best with a model in which both free monomers as well as trimers are present (Figure 5A), suggesting a weak but specific interaction. If we make the assumption that there is a monomer−trimer equilibrium, with no dimeric intermediates, we can calculate an apparent monomer−trimer dissociation constant of around 2.5×10^{-9} M^2, relative to an apparent monomer−trimer dissociation constant of around 9.8×10^{-12} M^2 for Kl-t75 (Figure 5B). Kl-t75 also appears to form hexamers at high protein concentrations, with an apparent trimer−hexamer dissociation constant of around 1.4×10^{-15} M^3.

The C-terminal helix B is represented by the synthetic peptide pepC3. This peptide shows a surprising degree of

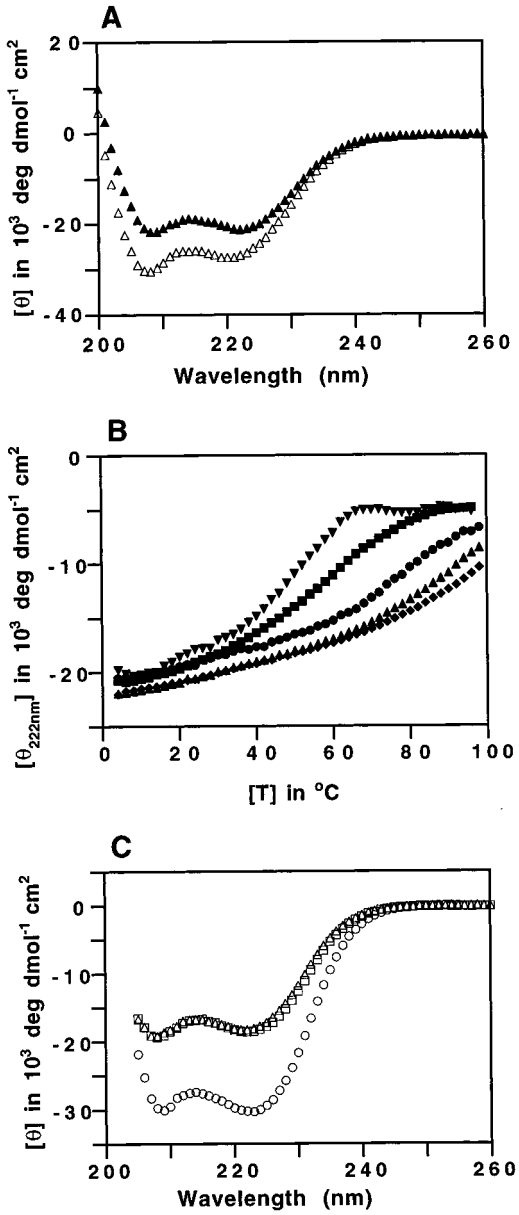

FIGURE 6: Secondary structure contributions of helix B. (A) Circular dichroism spectrum of pepC3 at 50 μM in standard C/P buffer (▲) and in buffer with 50% trifluoroethanol (△). (B) Concentration dependence of the thermal stability of pepC3 in standard C/P buffer as measured by circular dichroism at Θ_{222}. Concentrations of pepC3 are 5 μM (▼), 10 μM (■), 20 μM (●), 50 μM (▲), and 100 μM (◆). (C) Circular dichroism spectra of Kl-t75 z2bg (□) and Kl-t75z2,3bg (△) shown in comparison to wild-type Kl-t75 (○) at 20 uM C/P buffer.

secondary structure under mild conditions (20 μM monomer concentration, C/P buffer, pH 8.0, 4 °C). The helical content as measured by CD spectroscopy is 62%, which increases only slightly to 81% upon addition of trifluoroethanol (TFE) to 50% (Figure 6A). This suggests that the isolated subdomain is already well folded. Thermal melts show a concentration dependence of the melting point, suggesting that the peptide associates in the micromolar concentration range (Figure 6B). However, the thermal unfolding transitions are relatively shallow, indicating that the unfolding is not very cooperative; this behavior is typical for isolated subdomains (*34*). Sedimentation equilibrium studies also show that the peptide forms large oligomers in solution, with the average molecular weight larger than a hexamer, although this is somewhat dependent on starting conditions (data not shown).

Because pepC3 appeared to aggregate in solution, the role of helix B was further studied by mutating the hydrophobic residues of helix B within a background of the full-length protein Kl-t75. Helix B has two overlapping frames of hydrophobic repeats (Figure 1). Kl-t75 z2bg replaces the hydrophobic residues of the repeat in the same frame of reference as helix A (i.e., zipper 2 "be gone"), while Kl-t75 z2,3bg replaces the hydrophobic residues from both overlapping repeats (i.e., zipper 2 and 3 "be gone"). Both mutants have reduced α-helicity compared to Kl-t75 (Figure 6C). In addition, the Kl-t75 mutants have apparent monomer−trimer dissociation constants of around 5.3×10^{-10} M^2 (data not shown), which are closer in value to the dissociation constant for Kl-t59 than Kl-t75 (Figure 5). The Kl-t75 mutants also show no evidence of hexamer formation, similar to Kl-t59, supporting the contention that helix B, which can form hexamers, has been effectively mutated in these constructs.

DISCUSSION

In this paper, we have elaborated on our model of the structure of the trimerization domain of *K. lactis* HSF (*5*). Initially, we delineated the boundaries of this domain, using partial proteolysis and a series of truncations. The results for the C-terminal boundary of the trimerization domain supported our expectations from sequence analysis: protease susceptible sites immediately distal to the C-terminus of the heptad repeats of helix B are cut, while potential sites within the heptad repeats of helices A and B are protected. In addition, three thermolysin sites N-terminal to the heptad repeat of helix A are also protected, suggesting that parts of the polypeptide chain beyond the immediate heptad repeats are important for the structure of the domain. This contention is supported by the fact that Kl-t65, a peptide lacking the first 10 N-terminal residues, has no detectable secondary structure.

Next, we examined the overall topology of the trimerization domain in solution. To determine the orientation of the subunits, we used ^{19}F NMR spectroscopy of fluorinated residues incorporated at two positions of the heptad repeat. The premise of this experiment is that a parallel three-stranded coiled-coil structure would result in an identical environment for a given residue in all three subunits of the trimer. Since the chemical shift of a ^{19}F nuclear spin is very sensitive to its enviroment, the number of signals in the ^{19}F NMR spectrum of a specifically labeled fragment of the trimerization domain should indicate the number of different environments for the three subunits. Indeed, Kl-t75 with either a fluorinated tyrosine residue at position 326 or a fluorinated tryptophan residue at position 346 shows only a single peak in its ^{19}F NMR spectrum, suggesting that those residues are exposed to the same environment in all three subunits. One possible caveat for this interpretation is the postulated location for residue Y326 in position *f* based on the heptad repeat, placing it on the outside face of the helix opposite to the contact interface between the subunits. It is therefore possible that this residue might not interact strongly enough with the electrical fields of the other subunits to show a noticeable interhelix influence on the chemical shift. Nevertheless, W346, postulated to be in position *e*, should

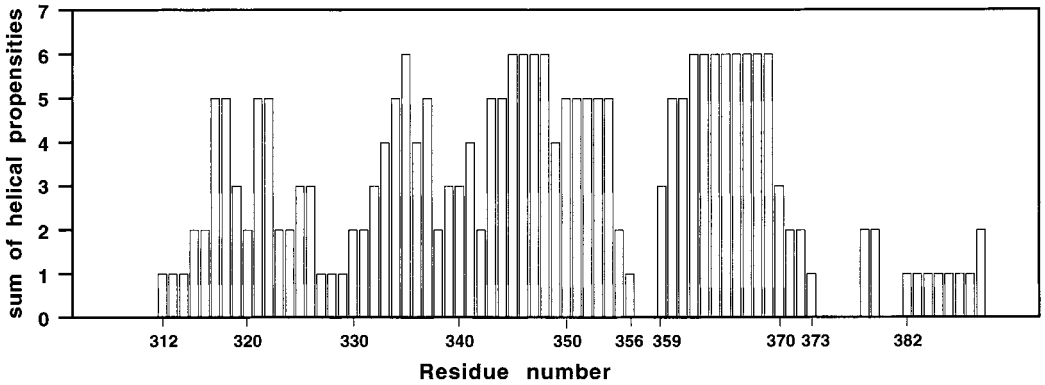

FIGURE 7: Secondary structure prediction of HSF trimerization domains. The program nnPredict was used to predict the secondary structure of the HSF trimerization domains from *K. lactis*, *S. cerevisiaie*, *Schizosaccharomyces pombe*, and *Drosophila melanogaster*, as well as the two mammalian HSFs, mHSF1 and mHSF2 (*12, 49*−*53*). The plot shows the number of cases in which a given position is predicted to be helical (i.e., sum of helical propensities). The position number is given relative to the residue within the *K. lactis* HSF sequence.

be partially buried in the cleft formed by the helices, a hypothesis supported by the limited accessibility of this residue to small molecules in fluorescence quenching assays (data not shown) and its slightly increased line width with respect to the fY326 resonance. Since this residue clearly shows only a single chemical shift, it seems likely that all three tryptophan residues in the trimer are exposed to the same environment. This rules out any antiparallel arrangement of the subunits, as well as any shift of the subunits relative to each other along the long axis of the trimer (i.e., any change in register).

The overall fold of the domain was then elucidated by using EPR spectroscopy to determine inter- and intrasubunit distances. In a first experiment, the distance between the C-termini of the subunits in the trimer was determined to be approximately 13−14 Å. This value is within the range of distances between identical residues in the subunits of a three-stranded coiled-coil, such as the trimeric mutant form of the GCN4 leucine zipper, where distances range between 11.5 and 16.2 Å (*35*). While close packing of the spin-labels against the coiled-coil could still lead to distances compatible with the distances determined by EPR, the fact that the labels show no motional restraint rules out this possibility. The hypothesis of intrasubunit interactions between helices A and B was also addressed by using a doubly labeled fragment with labels at residue 346 (in the C-terminal third of helix A) and at the C-terminus of the fragment (at the end of helix B). Both residues are at a similar distance from the region between helices A and B, which is the most likely candidate to act as a joint between a central coiled-coil and buttressing helix, as is found in viral envelope glycoproteins (*16, 21*). Nevertheless, no interaction was detected, supporting strongly the model in which the trimerization domain has an elongated structure with no interactions between helices A and B.

This model of an elongated structure is in disagreement with our previously published model of the trimerization domain (*5*). Although our previous analytical ultracentrifugation data correctly estimated that the proper shape of the trimerization domain was a prolate ellipsoid (i.e., a rodlike, elongated shape with one long semi-axis of length '*a*' and two short semi-axes of length '*b*') (*5*), we had made a simple mathematical error when calculating the semi-axial ratios for Kl-t96 (*36*). Our new calculations for Kl-t96 give an axial ratio of around 6:1 (data not shown), which is consistent with an elongated structure. This is supported by data presented in this paper on the sedimentation velocity of Kl-t75, which shows that the correct semi-axial ratio of the prolate ellipsoid is close to 5:1 for the 75 amino acid fragment. Based on the crystal structures of both naturally occurring and designed three-stranded coiled-coils (*14, 19, 37, 38*), we can assume a short semi-axis of between 13 and 15 Å. This also agrees with the intersubunit measurement of 13−14 Å between C-termini in Kl-t75 cC. Considering the calculated volume, Kl-t75 should have a long semi-axis of between 65 and 75 Å, or a length of between 130 and 150 Å. This dimension is long enough to encompass an elongated, mostly helical structure of 75 amino acids.

Finally, we looked at the subdomain structure of the trimerization domain. Helices A and B were originally defined by sequence analysis (Figure 1). Our experimental data show that both subdomains have the potential to form coiled-coils independently. Kl-t59, representing helix A, was shown to form a trimer in solution (Figure 5A), although of lower stability than the complete Kl-t75 domain (Figure 5B). PepC3, the peptide based on the isolated helix B of the trimerization domain, is also helical and can form large oligomers in solution (Figure 6A). The fact that pepC3 strongly oligomerizes suggests that helix B is involved in stabilizing the trimerization domain. Indeed, mutation of hydrophobic repeats in helix B decreases the helicity for Kl-t75 (Figure 6C), as well as the dissociation constant for a monomer−trimer equilibrium relative to wild-type Kl-t75 (data not shown). Given that the independent subdomain A can form trimers in solution and that removal of subdomain B reduces the ability of Kl-t75 to form trimers, it is likely that both subdomains are critical and that they are trimeric and probably forming coiled-coils within the context of the isolated trimerization domain. In support of the idea of two independent subdomains is evidence from in vivo studies of *K. lactis* HSF whereby deletion of helix A leads to a different phenotype than deletion of helix B (*39*).

The strength of the Kl-t75 dissociation constant (9.8×10^{-12} M^2) can be compared to two other published values for dissociation constants of HSF. Using fluorescent quenching experiments, a dissociation constant of 3×10^{-10} M^2 was found for a fragment of *K. lactis* HSF containing the DNA binding domain and the trimerization domain ending at residue 385 (*40*). Gel filtration chromatography on full-length *D. melanogaster* HSF gave a dissociation constant of around 2.2×10^{-7} M^2 (*41*). Even accounting for

differences in technique and conditions, these results support our contention that Kl-t75 represents the isolated trimerization domain from *K. lactis*. The lower values for a *K. lactis* HSF fragment containing the DNA binding domain domain and trimerization domain might be due to steric interference of the DNA binding domain or to differences in the C-terminal truncation, while the even lower values for the *D. melanogaster* HSF support the predominance of monomeric HSF in higher eukaryotes under nonshocked conditions (*41*).

A question that still remains open concerns the structure of the region between helices A and B. Secondary structure analysis programs such as PHD (*42*) and nnPredict (*43*) do not predict this region to be helical. For example, Figure 7 illustrates the summation of the predicted helical propensity from the sequences of six HSF trimerization domains. The predicted helicity drops after residue 373 (using the *K. lactis* HSF sequences as a reference), in agreement with our C-terminal domain boundary. Between residues 356 and 359, there is a gap with no predicted helicity; this region is located within the postulated linker region between helices A and B. Although not definitive, this suggests that there might be a break in the helicity of the trimerization domain.

Another question that also has to be addressed is the relation between the structure of the isolated domain and its structure in the context of the full-length HSF. As the studies on the trimerization domain of influenza hemagglutinin have shown (*16*, *19*, *44*), significant rearrangements can occur in the topology of a domain. Considering the large number of hydrophobic residues in the *e* and *g* positions of helix B, as well as the large number of conserved residues in helix A, it seems possible that at least during some points of the functional cycle of HSF helices A and/or B might interact either with other domains of HSF or with other proteins. In support of this latter contention, recent results have identified proteins that interact directly with HSF's trimerization domain (*45*−*47*). Alternatively, the extra hydrophobic residues in helix B might be responsible for stabilizing large oligomers such as the hexamers that form when HSF forms DNA loops (*48*).

ACKNOWLEDGMENT

We thank the following people: Dr. Susan Marqusee, for use of her AVIV spectropolarimeter; Dr. Howard Schachman, for use of his Beckman XLA Ultracentrifuge; and Dr. James D. Lear, for analysis of the sedimentation equilibrium data.

REFERENCES

1. Wu, C. (1995) *Annu. Rev. Cell Dev. Biol. 11*, 441−469.
2. Amin, J., Ananthan, J., and Voellmy, R. (1988) *Mol. Cell. Biol. 8*, 3761−3769.
3. Xiao, H., and Lis, J. T. (1988) *Science 239*, 1139−1142.
4. Drees, B. L., Grotkopp, E. K., and Nelson, H. C. M. (1997) *J. Mol. Biol. 273*, 61−74.
5. Peteranderl, R., and Nelson, H. C. M. (1992) *Biochemistry 31*, 12272−12276.
6. Voellmy, R. (1994) *Crit. Rev. Eukaryotic Gene Expression 4*, 357−401.
7. Baler, R., Dahl, G., and Voellmy, R. (1993) *Mol. Cell. Biol. 13*, 2486−2496.
8. Sarge, K. D., Murphy, S. P., and Morimoto, R. I. (1993) *Mol. Cell. Biol. 13*, 1392−1407.
9. Jakobsen, B. K., and Pelham, H. R. (1988) *Mol. Cell. Biol. 8*, 5040−5042.
10. Liu, X. D., Liu, P. C. C., Santoro, N., and Thiele, D. J. (1997) *EMBO J. 16*, 6466−6477.
11. Sorger, P. K., and Nelson, H. C. M. (1989) *Cell 59*, 807−813.
12. Jakobsen, B. K., and Pelham, H. R. (1991) *EMBO J. 10*, 369−375.
13. Nover, L., Scharf, K.-D., Gagliardi, D., Vergne, P., Verner-Czarnaecka, E., and Gurley, W. B. (1996) *Cell Stress Chaperones 1*, 215−223.
14. Harbury, P. B., Zhang, T., Kim, P. S., and Alber, T. (1993) *Science 262*, 1401−1407.
15. Woolfson, D. N., and Alber, T. (1995) *Protein Sci. 4*, 1596−1607.
16. Wilson, I. A., Skehel, J. J., and Wiley, D. C. (1981) *Nature 289*, 366−373.
17. Yan, Y., Winograd, E., Viel, A., Cronin, T., Harrison, S. C., and Branton, D. (1993) *Science 262*, 2027−2030.
18. Lovejoy, B., Choe, S., Cascio, D., McRorie, D. K., DeGrado, W. F., and Eisenberg, D. (1993) *Science 259*, 1288−1293.
19. Bullough, P. A., Hughson, F. M., Skehel, J. J., and Wiley, D. C. (1994) *Nature 371*, 37−43.
20. Tao, Y., Strelkov, S. V., Mesyanzhinov, V. V., and Rossmann, M. G. (1997) *Structure 5*, 789−798.
21. Chan, D. C., Fass, D., Berger, J. M., and Kim, P. S. (1997) *Cell 89*, 263−273.
22. Studier, F. W., Rosenberg, A. H., Dunn, J. J., and Dubendorff, J. W. (1989) *Methods Enzymol. 185*, 60−89.
23. Kunkel, T. A. (1985) *Proc. Natl. Acad. Sci. U.S.A. 82*, 488−492.
24. Drees, B. L. (1995) Ph.D. Thesis, University of California, Berkeley.
25. Sambrook, J., Fritsch, E. G., and Maniatis, T. (1989) *Molecular Cloning: A Laboratory Manual*, Cold Spring Harbor Laboratory, Cold Spring Harbor, NY.
26. King, D. S., Fields, C. G., and Fields, G. B. (1990) *Int. J. Pept. Protein Res. 36*, 255−266.
27. Chen, Y.-H., Yang, J. T., and Martinez, H. M. (1972) *Biochem. J. 11*, 4120−4131.
28. Weast, R. C. (1975) *Handbook of Chemistry and Physics*, 59th ed., CRC Press, Cleveland.
29. Eisenberg, H. (1994) *Biophys. Chem. 53*, 57−68.
30. Brooks, I. S., Soneson, K. K., and Hensley, P. (1993) *Biophys. J. 64*, A244.
31. Rabenstein, M. D., and Shin, Y. K. (1995) *Proc. Natl. Acad. Sci. U.S.A. 92*, 8239−8243.
32. Millhauser, G. L., Fiori, W. R., and Miick, S. M. (1995) *Methods Enzymol. 246*, 589−610.
33. Cantor, C. R., and Schimmel, P. R. (1980) *Biophysical Chemistry*, Part II, W. H. Freeman and Company, San Francisco, CA.
34. Lumb, K. J., Carr, C. M., and Kim, P. S. (1994) *Biochemistry 33*, 7361−7367.
35. Gonzalez, L., Jr., Brown, R. A., Richardson, D., and Alber, T. (1996) *Nat. Struct. Biol. 3*, 1002−1009.
36. Peteranderl, R. (1995) Ph.D. Thesis, University of California, Berkeley.
37. Harbury, P. B., Kim, P. S., and Alber, T. (1994) *Nature 371*, 80−83.
38. Ogihara, N. L., Weiss, M. S., Degrado, W. F., and Eisenberg, D. (1997) *Protein Sci. 6*, 80−88.
39. Chen, Y., Barlev, N. A., Westergaard, O., and Jakobsen, B. K. (1993) *EMBO J. 12*, 5007−5018.
40. Drees, B. L., Rye, H. S., Glazer, A. N., and Nelson, H. C. M. (1996) *J. Biol. Chem. 271*, 32168−32173.
41. Zhong, M., Orosz, A., and Wu, C. (1998) *Mol. Cell 2*, 101−108.
42. Rost, B., Sander, C., and Schneider, R. (1994) *Comput. Appl. Biosci. 10*, 53−60.
43. Kneller, D. G., Cohen, F. E., and Langridge, R. (1990) *J. Mol. Biol. 214*, 171−182.
44. Carr, C. M., and Kim, P. S. (1993) *Cell 73*, 823−832.

45. Yoshima, T., Yura, T., and Yanagi, H. (1997) *Biochem. Biophys. Res. Commun. 240*, 228−233.
46. Yoshima, T., Yura, T., and Yanagi, H. (1998) *Gene 214*, 139−146.
47. Satyal, S. H., Chen, D., Fox, S. G., Kramer, J. M., and Morimoto, R. I. (1998) *Genes Dev. 12*, 1962−1974.
48. Wyman, C., Grotkopp, E., Bustamante, C., and Nelson, H. C. M. (1995) *EMBO J. 14*, 117−123.
49. Sorger, P. K., and Pelham, H. R. (1988) *Cell 54*, 855−864.
50. Wiederrecht, G., Seto, D., and Parker, C. S. (1988) *Cell 54*, 841−853.
51. Gallo, G. J., Prentice, H., and Kingston, R. E. (1993) *Mol. Cell. Biol. 13*, 749−761.
52. Clos, J., Westwood, J. T., Becker, P. B., Wilson, S., Lambert, K., and Wu, C. (1990) *Cell 63*, 1085−1097.
53. Sarge, K. D., Zimarino, V., Holm, K., Wu, C., and Morimoto, R. I. (1991) *Genes Dev. 5*, 1902−1911.

BI981774J